



OPEN

Green synthesis and characterization of Fe₃O₄ nanoparticles using *Chlorella*-K01 extract for potential enhancement of plant growth stimulating and antifungal activity

Theint Theint Win^{1,2}, Sikandar Khan³, Bo Bo², Shah Zada⁴ & PengCheng Fu^{1✉}

The purpose of this research was to determine the efficacy of iron oxide nanoparticles (Fe₃O₄-NPs) using microalgal products as a plant growth stimulant and antifungal agent. The work was conducted with the phyco-synthesis and characterization of Fe₃O₄-NPs using 0.1 M ferric/ferrous chloride solution (2:1 ratio; 65 °C) with aqueous extract of the green microalga *Chlorella* K01. Protein, carbohydrate and polyphenol contents of *Chlorella* K01 extract were measured. The synthesized microalgal Fe₃O₄-NPs made a significant contribution to the germination and vigor index of rice, maize, mustard, green grams, and watermelons. Fe₃O₄-NPs also exhibited antifungal activity against *Fusarium oxysporum*, *Fusarium tricinctum*, *Fusarium maniliforme*, *Rhizoctonia solani*, and *Phythium* sp. Fourier transform infrared spectroscopy (FTIR), X-ray diffraction (XRD), X-ray photoelectron spectroscopy (XPS) scanning electron microscopy (SEM), transmission electron microscopy (TEM), particle size analysers (PSA), and zeta potential (ZP) measurements were used to characterize these green fabricated magnetite NPs. FTIR analysis showed that the synergy of microalgal proteins, carbohydrates and polyphenols is responsible for the biofabrication of iron nanoparticles. A spheroid dispersion of biosynthesized Fe₃O₄-NPs with an average diameter of 76.5 nm was produced in the synthetic process.

Iron (Fe) is a nutrient that is required by all life forms, yet its deficiency is prevalent in many different crops^{1,2}. Iron plays a variety of important roles in plants, including the biosynthesis of chlorophyll, respiration, and the regulation of redox reactions^{3,4}. Crops growing on soil that are Fe-deficient lead to crops that are Fe-deficient which reduces yield and quality⁵. On the other hand, in perspective of the food chain, Fe deficiency can lead to anaemia in living creatures⁶. In order to overcome this problem, inorganic-iron, chelated-iron fertilizer, and organic-iron, are currently used⁷. High cost and its absorption potential^{8,9} are drawback of currently used fertilizers, therefore, formulation of using Fe fertilizer need to be improved.

Recent advances in the study of biofertilizers in the field of algae biotechnology have been made. *Chlorella* sp. is widely accepted as a model microorganism for academic studies^{10–13}. Using algae-based biofertilizers, which offer substantial benefits to green agriculture, has proven advantageous, with three key goals: healthy environment, economic profits, and socioeconomic equity. These can be met through the applications of algal biofertilizers in sustainable agriculture¹⁴. Algal metabolites have been found to promote mineralization and plant–microbe symbiosis by providing nutrients to the soil microbial community¹⁵. Furthermore, addition of cyanobacterial filtrates to plant seeds is seen to increase the average germination¹⁶. Biogenic nanoparticles have proven to be

¹State Key Laboratory of Marine Resource Utilization in South China Sea, Hainan University, 58 Renmin Avenue, Haikou 570228, Hainan Province, China. ²Biotechnology Research Department, Ministry of Science and Technology, Kyaukse 05151, Myanmar. ³Department of Biotechnology, Shaheed Benazir Bhutto University, Sheringal, KP 18000, Pakistan. ⁴Beijing Key Laboratory for Bioengineering and Sensing Technology, Research Center for Bioengineering and Sensing Technology, School of Chemistry and Bioengineering, University of Science and Technology, Beijing 100083, China. ✉email: pcfu@hainanu.edu.cn

effective nanomaterial-based fungicides for the control of some plant fungal diseases¹⁷. They have the potential to be widely used in agriculture as biocontrol agents to promote sustainable agriculture¹⁸. The environmentally green chemistry approach thus provides a clean, nontoxic, and environmentally friendly method of producing NPs with a wide range of size, morphology, component, and physical and chemical properties¹⁹. Moreover, metal oxide nanoparticles are stable and are considered to be safe for humans²⁰.

The main purpose of this study was to synthesize iron (Fe) nanoparticles based on microalgae for agricultural purposes. Aqueous extracts of *Chlorella* K01 have been used to biosynthesize environmental friendly plant growth stimulants and anti-fungal Fe nanoparticles (Fe₃O₄-NPs).

Materials and methods

All chemicals used were of analytical reagent grade and purchased from Aladdin, China. *Chlorella* K01 was gifted by Professor Prezemyslaw Malec and Dr. Jan Burczyk from Jagiellonian University, Krakow, Poland.

Preparation of algal extract and determination of protein, carbohydrate and polyphenol contents. *Chlorella* K01 was cultivated in fresh KC medium at 25–40 (μE m⁻² s⁻¹). Start-up seed culture was done in 250 ml sterile flasks having 100 ml KC medium. To obtain biomass, it was subcultured in 500 ml flasks and then larger 1000 ml flasks. The culture was washed with water, freeze dried and stored. To prepare this extract, 100 ml of ultrapure water was heated at 60–70 °C with 0.1 g of algal powder. The raw extract algal was constantly agitated, then filtered and the obtained supernatant was used as the algal bioextract.

The kit #16-6002 Bao Ruyi (Beijing) Biotechnology Co., Ltd used the BCA method to determine protein concentrations (bicinchoninic acid)²¹. The BCA/copper complex absorbance was measured at 562 nm in a UV-Vis spectrophotometer. A 0.5 mg ml⁻¹ bovine serum albumin standard curve was used to calculate protein concentration. The total phenolic content of the extracts calculated by using the Folin-Ciocalteu method²², gallic acid was the standard. The carbohydrate content was estimated using the phenol-sulfuric acid method. The absorbance at 490 nm was measured the colored aromatic complex formed between the phenol and the carbohydrate with glucose as a standard.

Synthesis of *Chlorella* K01 based Fe₃O₄ NPs. 0.1 M FeCl₂·4H₂O and 0.1% algal extract were added in the ratio 2:3, under four different pH conditions. NaOH was used to adjust the pH to 6, 8, 10, and 12. These reactions were kept at 60–70 °C. The synthesized Fe₃O₄-NPs were washed three times with 70% ethanol and dried in a hot air oven for 24 h. These iron oxide NPs were synthesized and stored until further use. The effects of germination on various Fe₃O₄-NPs seeds synthesized at different pH levels have been examined as shown in “Seed treatment and in vitro seed germination test” section.

Seed treatment and in vitro seed germination test. The commercialized seeds (rice, maize, mustard, green grams, and watermelons) were bought from the local Longhua market (20° 2' 9.672" N, 110° 20' 3.2634" E). All the seeds tested in the research are permitted and legal for trade, commercialization in China. Therefore Specific permission was not needed from the Local Authority.

Germination at various Fe₃O₄-NPs concentrations was evaluated to determine plant toxicity, as described by Stampoulis et al.²³. Firstly, soak the seeds in 0.1% mercuric chloride for 3 min, and then rinse thrice with sterilized distilled water. The aseptic seeds were soaked in solution containing (synthesized nanoparticles 1 mg ml⁻¹, 5 mg ml⁻¹, 7 mg ml⁻¹, 10 mg ml⁻¹, bulk FeCl₂·4H₂O (0.1 M) Gibberellic acid (GA) 15 mg ml⁻¹) for 1 h and agitated at 100 rpm. The control was sterilized and treated with distilled water. Afterwards, all of the seeds were transferred to plates that contained two layers of wetted filter papers that were carefully rolled (25 seeds per plate) and incubated at 25 °C under a 16:8 (light: dark) cycle for 7 days. The germination percentage was calculated using normal seedlings. Ten seedlings from each replicate were chosen at random to be measured for shoot and root length. Triplicate experiment was repeated three times. For their comparative study, the vigor index was calculated for seeds throughout germination experiments that exhibit the best responses to Fe₃O₄, bulk FeCl₂·4H₂O (0.1 M), Gibberellic acid, and control. A vigor index was calculated as given by Abdul-Baki and Anderson²⁴:

$$\text{Vigor index I} = \text{Germination \%} \times \text{Seedling length (Root + Shoot)}^{25}$$

Anti-fungal activity against phytopathogens. The antifungal activity of Fe₃O₄-NPs was examined against the fungal pathogens; *Fusarium oxysporum*, *Fusarium tricinctum*, *Fusarium maniliforme*, *Rhizoctonia solani*, and *Phythium* sp. Fungal cultures were incubated in potato dextrose media (PDA) liquid media at 26 °C for 5 days before being cultured on fresh PDA solid media with 1 × 10⁷ spores ml⁻¹. The agar well diffusion method²⁵ was used in this study. PDA medium was punched into 8 mm wells and 100 μl of Fe₃O₄-NPs at 1 mg ml⁻¹ were added. The plates were incubated at 26 °C for 5 days. For the experimental control, plates containing no Fe₃O₄-NPs were incubated under same conditions.

Characterization. The synthesized nanoparticles were characterized via, Fourier Transformed Infra-red Spectroscopy (FT-IR), X-ray Diffraction (XRD), X-ray photoelectron spectroscopy (XPS), Zeta potential, Dynamic light scattering (DLS), scanning electron microscope (SEM), and transmission electron microscopes (TEM).

Electron microscopy. On the carbon-coated copper grids, a drop of Fe₃O₄-NPs colloid (50 μl) was placed. TEM was used to examine the morphology and size of phylogenetic Fe₃O₄-NPs (TEM). TEM micrographs have been

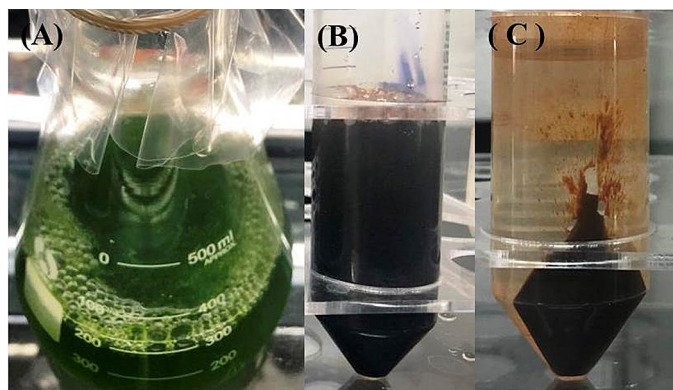


Figure 1. One month old *Chlorella* K01 culture (A) and synthesized Fe_3O_4 -NPs solution (B), Crude Fe_3O_4 -NPs (C).

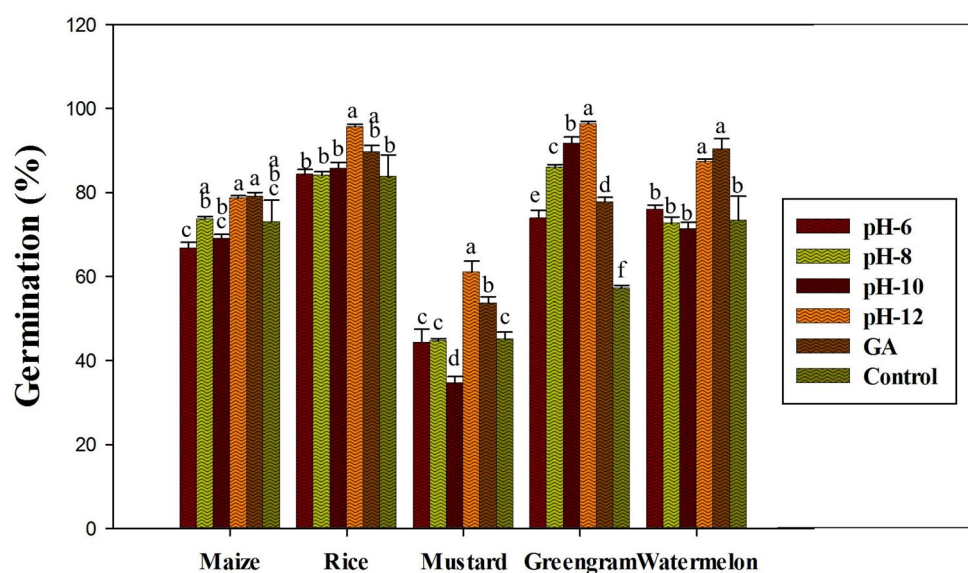


Figure 2. Germination of maize, rice, mustard, greengram and watermelon with different Fe_3O_4 -NPs synthesized by different pH. Data are mean \pm SD. Each group without sharing letter mean statistical significance ($P \leq 0.05$).

captured through the analysis of the prepared grids on an AMT camera system. The particle size was also determined by TEM using an Image Analyser System (IAS). The surface features of Fe_3O_4 -NPs deposited on a graphite grid were examined using a SEM (model S360 brand SEM—Leica Cambridge, Cambridge, UK).

X-ray diffraction (XRD) and X-ray photoelectron spectroscopy. Cu K α radiation was used to generate the x-ray diffraction (XRD) pattern, which was recorded using an X-ray diffractometer (Powder X-ray-D8 advanced diffractometer, Bruker) from 5 $^\circ$ to 100 $^\circ$ 2 θ angles at 40 kV and 30 mA. The exposure time was 300 s. Besides, X-ray photoelectron spectroscopy (Thermo Scientific ESCALAB 250) was used to further analyse the chemical composition and binding energies of the as prepared Fe_3O_4 nanoparticles²⁶.

Fourier transform infrared (FTIR) spectral analyses. The Fe_3O_4 -NPs colloid was biosynthesized and centrifuged at 10,000 g for 15 min after being lyophilized and grinded with potassium bromide (KBr) powder for FTIR measurements. The spectrum was captured in the 500–4000 cm^{-1} range using a Bruker, TGA-IR, TENSOR 27 spectrometer in diffuse reflectance mode with a resolution of 4 cm. In accordance with previously published information, spectral absorption bands were identified.

Zeta potential and dynamic light scattering (DLS). With the help of dynamic light scattering (DLS) and zeta potential (HORIBA Zetasizer SZ-100), the distribution and size of Fe_3O_4 -NPs were determined.



Figure 3. Germination characteristics of tested crops (A) corn, (B) rice, (C) mustard, (D) watermelon, (E) greengram.

Statistical analysis. Triplicated data of each experiment was analysed statistically using one-way analysis of variance (ANOVA); Minitab 17.1.0 (Minitab Pty, Sydney, Australia) and Excel software, and the mean values for each treatment were compared using the Turkey's test at the $P < 0.05$ confidence level.

Results and discussion

Iron oxide nanoparticles were successfully prepared using a green approach with microalgal extract in an alkaline medium. Fe_3O_4 -NPs was created using a microalgal extract in a quick, cost-effective, and environmentally safe way¹⁹. According to El-Kassas et al. (2017), proteins and polyphenols from *Chlorella* K01 catalyse the reduction of iron ions into nanoparticles, and polysaccharides stabilize Fe_3O_4 -NPs²⁷. *Chlorella* K01 extract contains $632 \pm 195 \text{ mg ml}^{-1}$ of protein, $39.59 \pm 3.04 \text{ mg ml}^{-1}$ of carbohydrate and $0.12 \pm 0.007\%$ of polyphenol content. Therefore, the extract can be used for the bio fabrication of Fe_3O_4 -NPs. 1 g of dry algal powder yielded 16 mg at pH-6, 645 mg at pH-8, 703 mg at pH-10 and 829 mg at pH-12 of Fe_3O_4 -NPs. Figure 1 illustrates one month old *Chlorella* K01 culture, aqueous Fe_3O_4 -NPs solution and Crude Fe_3O_4 -NPs.

According to the results of the in vitro germination test, Fe_3O_4 -NPs synthesized at pH-12 showed significantly higher germination rates ($P \leq 0.05$) and was therefore used for further investigation (Fig. 2). The description of the crops used in this experiment, as well as their germination activity, is shown in Fig. 3. In terms of the effect of different Fe_3O_4 -NPs concentrations on seed germination, Fe_3O_4 -NP-treated seeds (1 mg ml^{-1}) had a higher germination rate, a higher vigor index, and a notable increase in seedling shoot and root formations ($P \leq 0.05$) among the crops than GA treated seeds and control seed (Figs. 4, 5). When compared to the positive and negative control seedlings, the Fe_3O_4 -NPs treatments had a higher germination rate, root length, and vigor index ($P \leq 0.05$). Among the crops tested, green gram demonstrated the most remarkable plant growth and vigor index (Figs. 3, 5). Fe nanoparticles have been shown to have a negative effect on the germination process and germination parameters of sunflower seedlings²⁵. Few reports on the effects of Fe-NPs in plants are available,

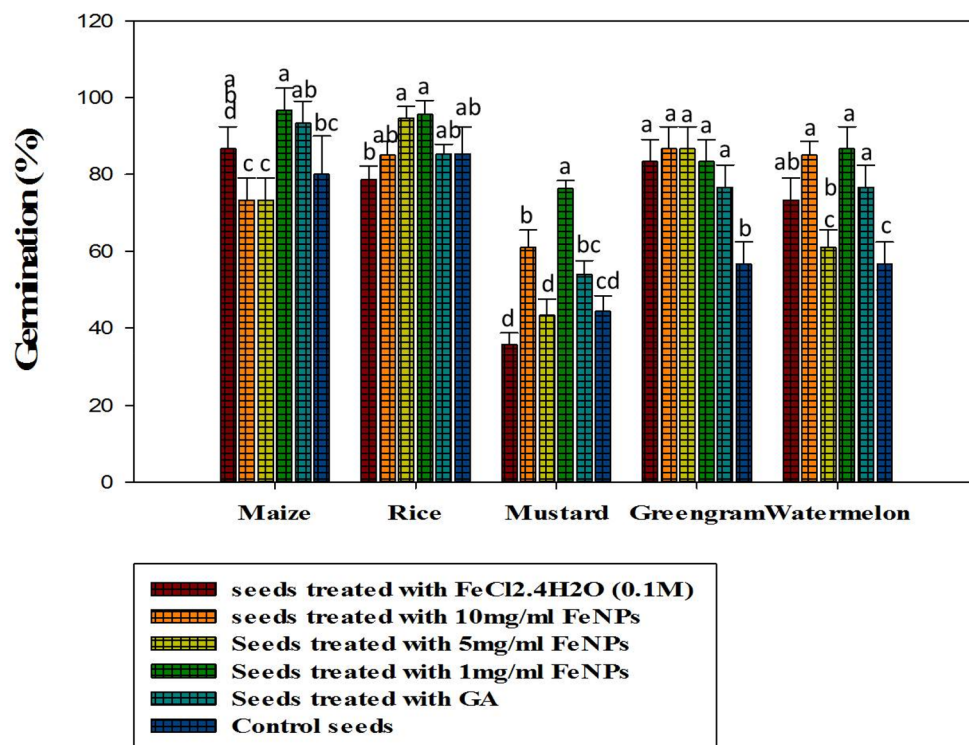


Figure 4. Percentage of seed germination in vitro condition with different doses of Fe₃O₄-NPs synthesized by pH-12. Data are mean ± SD. Each group without sharing letter mean statistical significance ($P \leq 0.05$).

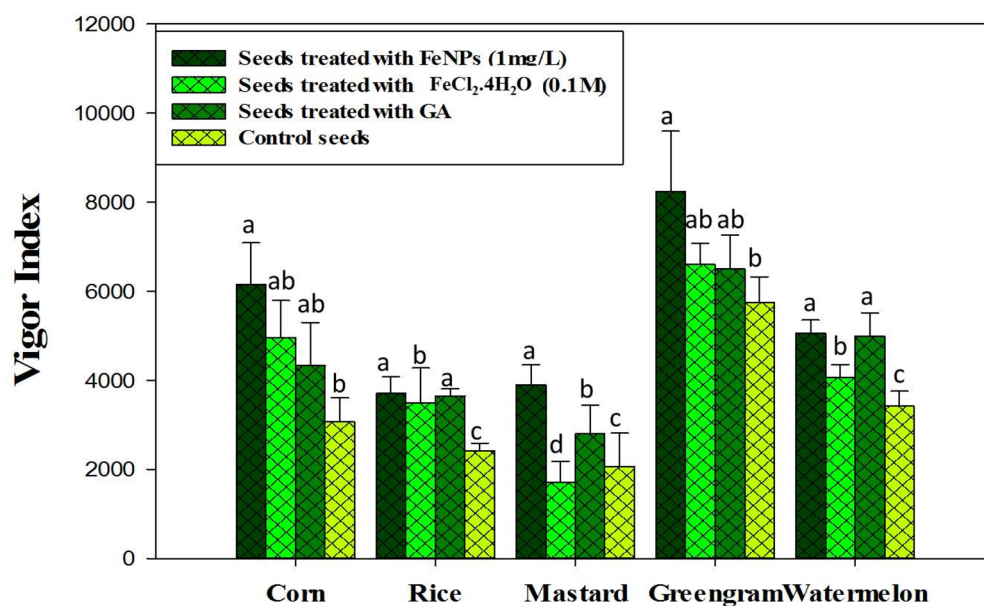


Figure 5. Effect of Fe₃O₄-NPs, bulk FeCl₂.4H₂O (0.1 M), and Gibberellic acid on Vigor index of the tested crops. Values in each bar are represented as mean ± SD.

Shankamma et al.²⁸ stated that the research outcomes depend on the nature of the NPs and plant species and are not always consistent with each other. However, the crops in this study showed no negative effects during germination with varying concentrations of Fe₃O₄-NPs. This is due to the reaction of plant growth stimulant microalgae metabolites with FeCl₂¹⁴. This is consistent with the findings of Ilona et al. (2019), who found that Fe₃O₄-NPs at concentrations of 1 mg L⁻¹, 2 mg L⁻¹, and 4 mg L⁻¹ induce low genotoxicity and have a beneficial effect on the growth and development of rocket seedlings, implying that nanoparticles may improve plants'

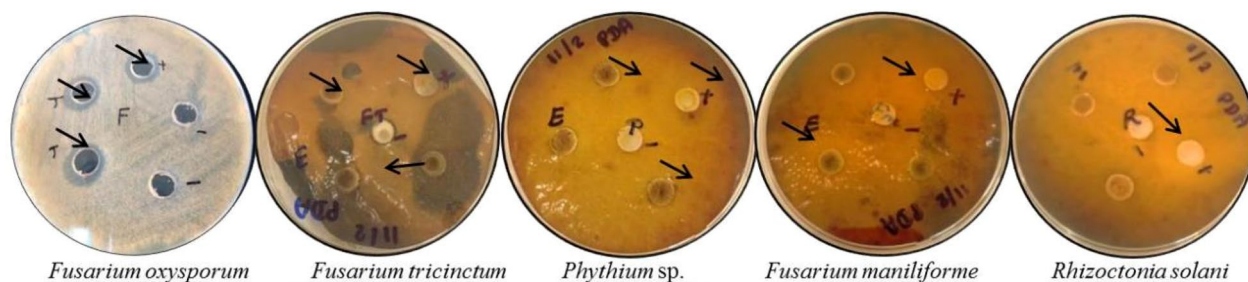


Figure 6. Antifungal zone of inhibition by iron oxide (Fe_3O_4) nanoparticles (From left to right) *Fusarium oxysporum*, *Fusarium tricinctum*, *Phythium* sp. *Fusarium maniliforme*, and *Rhizoctonia solani*.

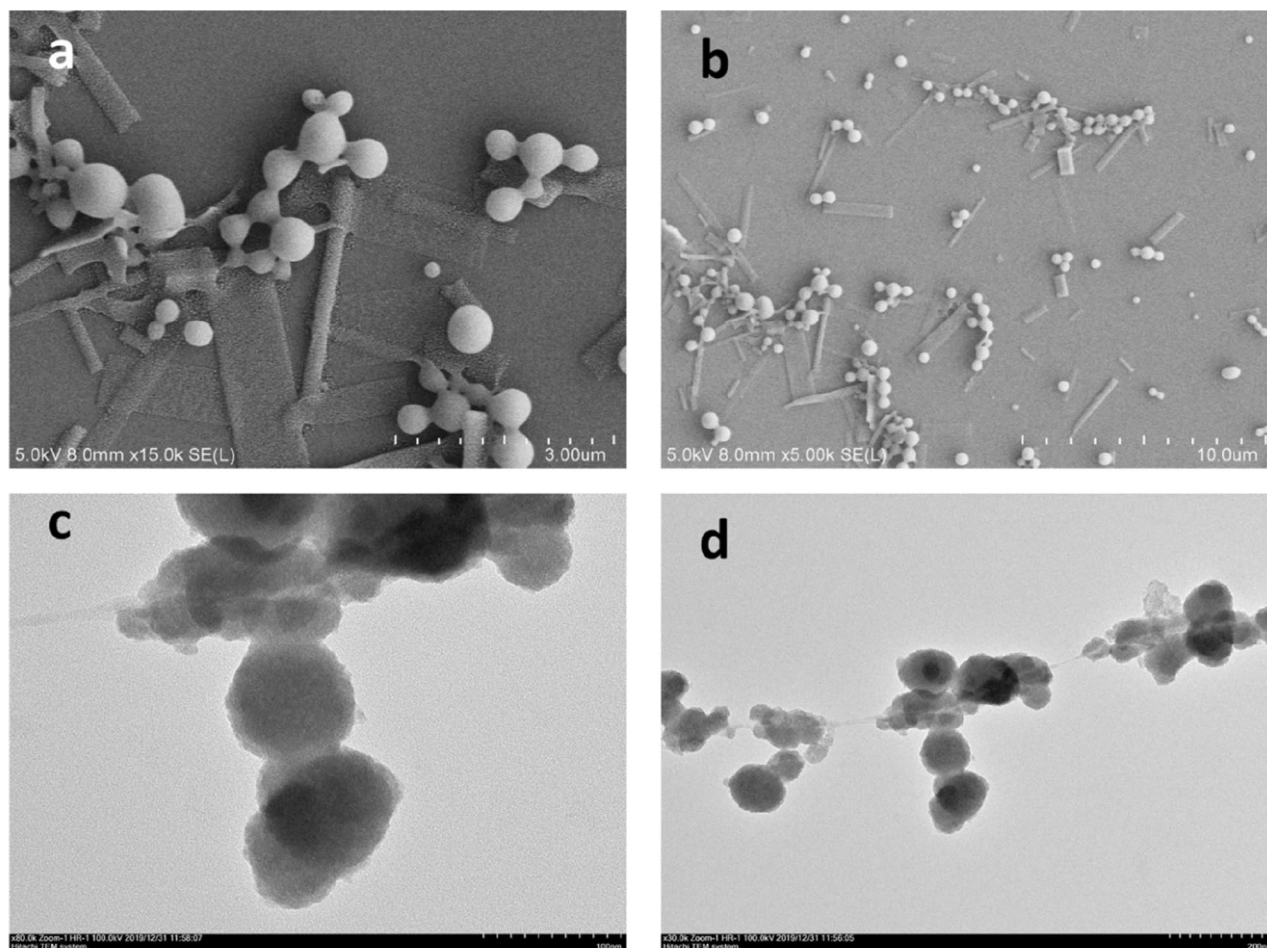


Figure 7. SEM (“a” and “b”) and TEM (“c” and “d”) images of the as prepared Fe_3O_4 -NPs using *Chlorella* K01 extracts as capping and reducing agents.

resistance to environmental stresses²⁹. Polischuk et al. (2019) also noted that Fe_3O_4 -NPs treatment increased 10% in seed germination compared to the control, as well as a 25–30% increase in root growth³⁰. On the other hand, González-Melendi et al. (2008) and Zhu et al. (2008) searched into Fe-oxides and found that they are relatively safe for nanoparticle delivery in plants^{31,32}.

Qualitative assessment of antifungal activity against *Fusarium oxysporum*, *Fusarium tricinctum*, *Fusarium maniliforme*, *Rhizoctonia solani*, and *Phythium* sp. growth were carried out. All tested fungal growth showed inhibition when treated with Fe_3O_4 -NPs. Each phytopathogen had an inhibition zone diameter ranging from 10 to 25 mm (Fig. 6). The results clearly demonstrate that iron oxide nanoparticles at the concentrations used in this study (1 mg L^{-1}) showed the inhibition of radial growth of all fungal pathogens tested. The appearance of an inhibition zone on culture media demonstrates the iron oxide nanoparticles’ biocidal activity³³. Additionally, Nehra et al. (2017) demonstrated that iron oxide nanoparticles have antifungal and antibacterial activity. As a result, they concluded that iron oxide nanoparticles can be effectively used as antimicrobial agents³⁴.

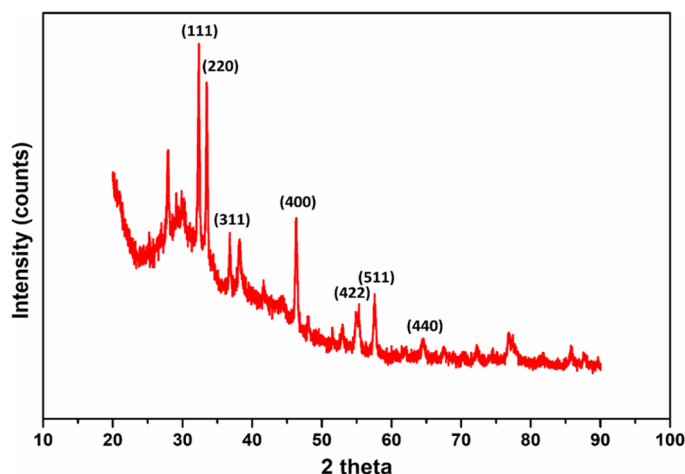


Figure 8. XRD pattern of the biosynthesized Fe_3O_4 -NPs.

Morphological study of Fe_3O_4 -NPs was conducted using both the scanning and transmission electron microscopy (Fig. 7). It can be observed in the SEM images that the *Chlorella* K01 extracts mediated synthesis of Fe_3O_4 -NPs in a monodispersed form that are spherical in shape, and which are well separated without any evident aggregation (Fig. 7a,b). This excellent dispersion and spherical morphology of the NPs can be ascribed to the outstanding capping ability of the biochemical in the extracts of *Chlorella* K01. TEM analysis revealed the size and morphology of the synthesized NPs. The spherical biofabricated Fe_3O_4 -NPs were in the range of approximately 50 to 100 nm in size (Fig. 7c,d).

By employing an X-ray diffraction technique, we were able to determine the crystalline structure of the biofabricated Fe_3O_4 -NPs. The XRD profile of the biofabricated Fe_3O_4 -NPs is illustrated in Fig. 8. The XRD pattern of the Fe_3O_4 -NPs depict various spectral peaks at 2-theta = 31.2°, 33.6°, 36.2°, 46°, 54.8°, 57.1°, and 64°, that can be ascribed to their relevant indices and diffraction planes (111), (220), (311), (400), (422), (511), and (440), respectively. The diffraction planes of the current Fe_3O_4 -NPs are very much similar to that reported earlier for Fe_3O_4 -NPs³⁵.

X-ray photoelectron spectroscopy was conducted to confirm the synthesis of Fe_3O_4 nanoparticles and to analyze their oxidation states (Fig. 9). The XPS survey spectrum of Fe_3O_4 nanoparticles synthesized by *Chlorella* K01 extracts, showed the presence of Fe, O, C, and N (Fig. 9A). This full-scan resulted in to the high resolution subsequent spectra acquisition. The data was fitted, using the “XPSPEAK4.1” program available at <https://xpspeak.software.informer.com/4.1>. The two peaks in Fe2p for Fe_3O_4 -K01 extract sample, at approximately 714 eV and 723.5 eV can be ascribed to the binding energies of Fe^{3+} oxidation state of iron while the peak around 710.6 eV can be attributed to the binding energy of Fe^{2+} (Fig. 9B). Almost similar peak areas of the two Fe^{3+} peaks in the Fe2p XPS spectrum, indicates the synthesis of magnetite nanoparticles (Fe_3O_4)³⁶. The deconvolution of the O1s spectrum exhibited valuable information regarding the chemical states of oxygen linkage in the as prepared Fe_3O_4 (Fig. 9C). One peak at 531 eV is associated with the lattice oxygen (O in Fe–O–H), whereas the second peak at 530.1 eV can be attributed to the oxygen in Fe–O. The third peak illustrated in the O1s spectrum with binding energy of 529.6 eV is comparable to that observed in the literature as X=O (where X can be any active component in the biomolecule) and may be a by-product generated during the biosynthesis of Fe_3O_4 nanoparticles using *Chlorella* K01 extracts. These binding energies are due to the interactions between the Fe and the oxygen containing functional groups in the biological system. The bioactive materials containing these functionalities can react metal ions through ion exchange reactions, hence producing metal oxides (Fe_3O_4 in this case) nanoparticles. For the C1s XPS spectrum, the existence of peaks at binding energies 284.6 eV, 285 eV, 286.4 eV and 288.5 eV can be attributed to (C–C), (C–N), (C–O) and (C=O) linkages, respectively (Fig. 9D). Furthermore, the N1s XPS spectrum of Fe_3O_4 -K01 can be deconvoluted into two component peaks, namely pyrrolic nitrogen (400.1 eV) and nitrogen associated with carbon in the form of C–N at binding energy 399.5 eV (Fig. 9E). Similar findings have also been reported by Khan et al.³⁷.

The FTIR analysis was carried out in order to classify the functional groups in biomolecules extracted from *Chlorella* K01 that were utilized for the reduction and capping of the Fe_3O_4 -NPs (Fig. 10). The spectral bands at wave number 3710 cm^{-1} and 2815 cm^{-1} are more prominent as compared to others at 2255 cm^{-1} , 2550 cm^{-1} , and 3410 cm^{-1} . The active and prominent band at 3710 cm^{-1} confirmed the presence of O–H stretching indicating the polyphenolic group. The second dominant band at 2815 cm^{-1} can be ascribed to C–H stretching of aldehyde functional group. The other bands observed at 2255 cm^{-1} , 2550 cm^{-1} , and 3410 cm^{-1} correspond to $\text{C}\equiv\text{C}$, S–H, and N–H stretching vibrations which illustrate the presence of alkyne, thiol and primary amine functional groups, respectively. These results suggested that the extract of *Chlorella* K01 containing afore mentioned functional groups are involved in the reduction of FeCl_2 in Fe_3O_4 -NPs. Various earlier reports are in line with the current findings where they have reported amine, hydroxyl, carboxylic and phosphate functional groups in algal extracts are involved in the biofabrication of metal nanoparticles³⁸.

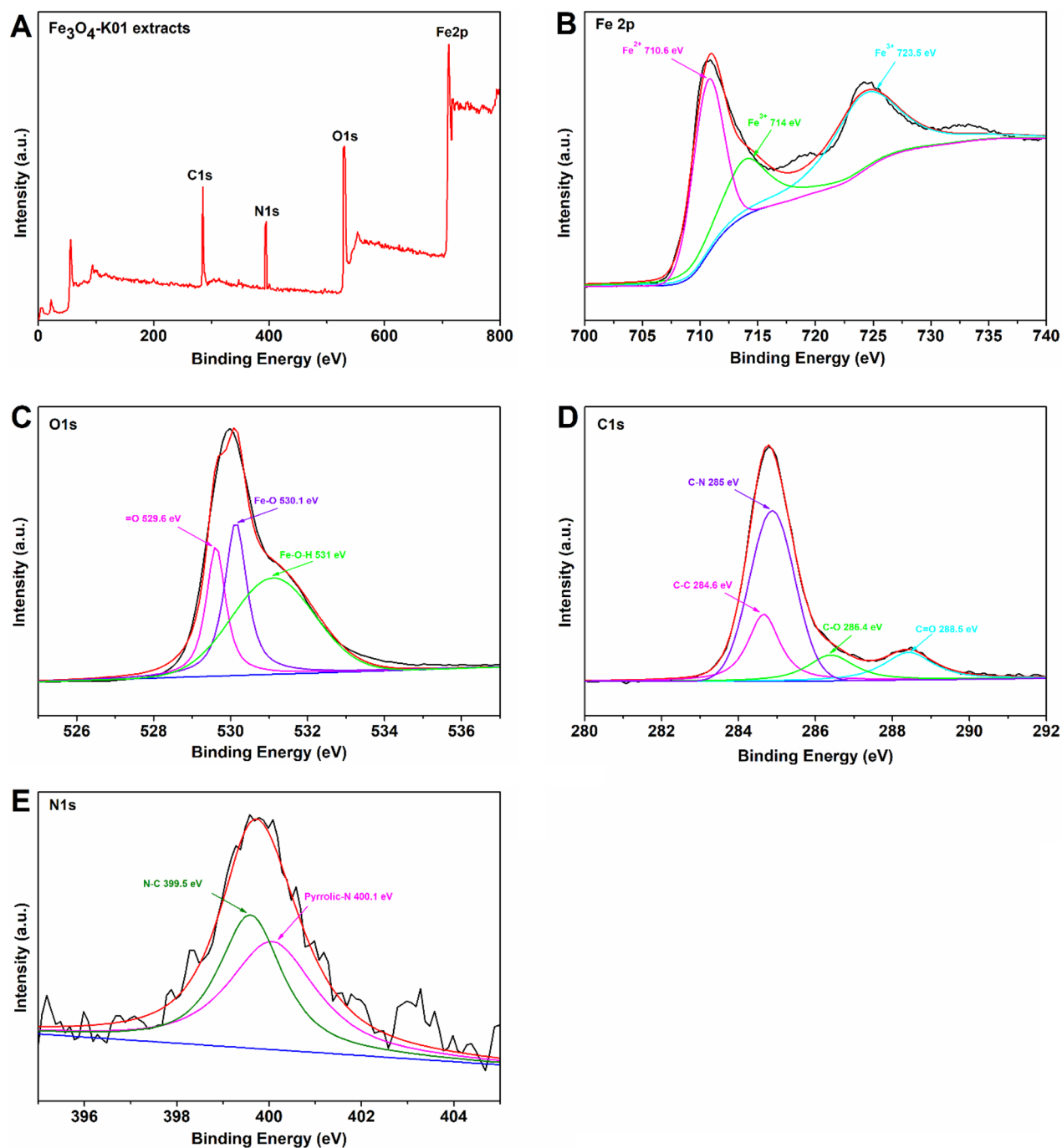


Figure 9. X-ray photoelectron spectra (XPS) of Fe_3O_4 -K01 extracts. Survey scan XPS spectrum (A), Fe 2p (B) O1s (C), C1s (D) and N1s (E) spectra of the K01 extracts based synthesis of Fe_3O_4 nanoparticles. The black lines (little noisy) denote experimental raw data, the overlaid red line is the deconvoluted form of raw data (sum of all fitting data), the baseline is presented by blue color and other color lines are the fitting data.

The zeta potential of the biofabricated Fe_3O_4 -NPs was observed as a sharp single peak in the range of -48 and 0 mV, having a maximum intensity at -25.8 mV (Fig. 11a). This suggested that the surface of Fe_3O_4 -NPs consists of negatively charged moieties that expanded in the medium. The dispersion of the NPs might be due to repulsive nature of the negative values which also suggested stability of the Fe_3O_4 -NPs. Lower values of zeta potential depict minimum or no flocculation and reduced tendency towards assembly.

DLS analysis reveals the particle size and distribution in the materials. DLS of the biofabricated Fe_3O_4 -NPs illustrate a particle size range of 20 to 200 nm (Fig. 11b). It was found that the average particle size of the Fe_3O_4 -NPs was 76.5 nm. The particle size and distribution identified via DLS analysis is consistent with that measured by SEM and TEM analysis.

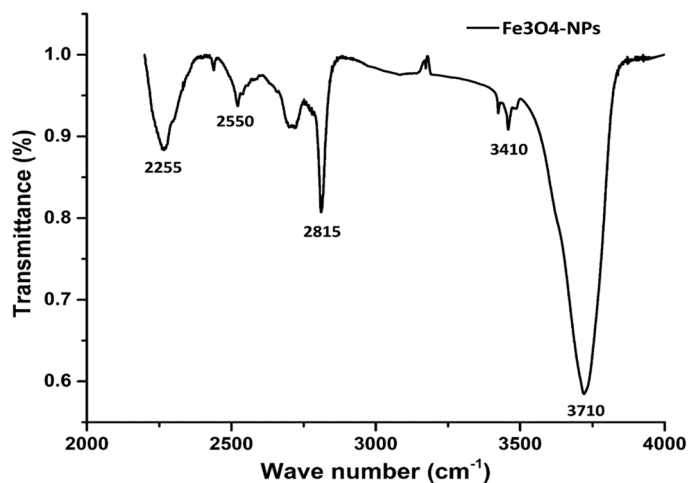


Figure 10. FTIR spectral analysis of the biofabricated Fe_3O_4 -NPs.

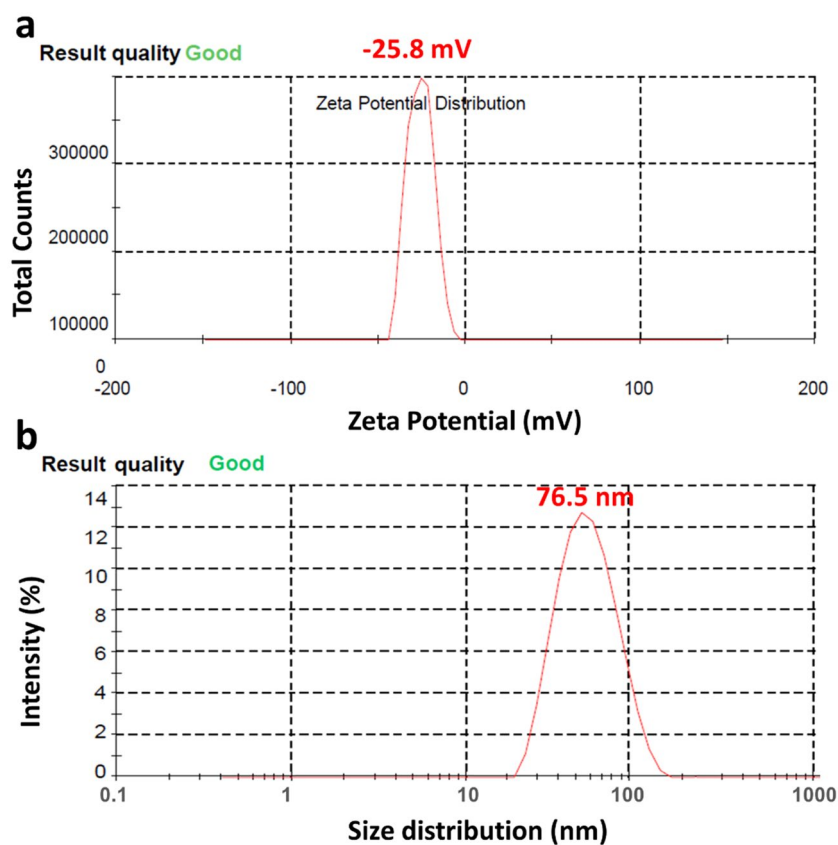


Figure 11. Zeta potential (a) and dynamic light scattering (b) of the biofabricated Fe_3O_4 -NPs, depicting the surface charge values and particle size distribution, respectively.

Conclusions

Iron oxide nanoparticles were generated using microalgal extract as a reducing agent. This method offers a simple yet environmentally friendly approach. When compared to other biological extracts previously reported, *Chlorella K01* was found to be more effective, as the NPs obtained with this extract have the lowest zeta potential (-25.8 mV) and the average particle size of the Fe_3O_4 -NPs was 76.5 nm. Iron oxide nanoparticles synthesized using this method showed promising plant growth stimulant and antifungal activities against a variety of fungal pathogens, and thus can be used to control a variety of fungal diseases. The Fe_3O_4 -NPs drastically enhanced rice, corn, mustard, green gram, and watermelon germination.

Received: 25 July 2021; Accepted: 26 October 2021

Published online: 09 November 2021

References

- Zuo, Y. & Zhang, F. Soil and crop management strategies to prevent iron deficiency in crops. *Plant Soil* **339**, 83–95 (2011).
- Sánchez-Alcalá, I. *et al.* Evaluation of preflooding effects on iron extractability and phytoavailability in highly calcareous soil in containers. *J. Plant Nutr. Soil Sci.* **177**, 150–158 (2014).
- Mimmo, T. *et al.* Rhizospheric organic compounds in the soil–microorganism–plant system: Their role in iron availability. *Eur. J. Soil Sci.* **65**, 629–642 (2014).
- Ye, L. *et al.* MPK3/MPK6 are involved in iron deficiency-induced ethylene production in Arabidopsis. *Front. Plant Sci.* **6**, 953 (2015).
- Kobayashi, T. & Nishizawa, N. K. Iron uptake, translocation, and regulation in higher plants. *Annu. Rev. Plant Biol.* **63**, 131–152 (2012).
- Li, X. *et al.* Bt-transgenic cotton is more sensitive to CeO₂ nanoparticles than its parental non-transgenic cotton. *J. Hazard. Mater.* **274**, 173–180 (2014).
- Laurie, S. H. *et al.* Influence of complexation on the uptake by plants of iron, manganese, copper and zinc: II. Effect of DTPA in a multi-metal and computer simulation study. *J. Exp. Bot.* **42**, 515–519 (1991).
- Cesco, S. *et al.* Solubilization of iron by water-extractable humic substances. *J. Plant. Nutr. Soil Sci.* **2000**(163), 285–290 (2000).
- Lucena, J. J., Gárate, A. & Villén, M. Stability in solution and reactivity with soils and soil components of iron and zinc complexes. *J. Plant. Nutr. Soil Sci.* **173**, 900–906 (2010).
- Doğan-Subaşı, E. & Demirel, G. N. Anaerobic digestion of microalgal (*Chlorella vulgaris*) biomass as a source of biogas and biofertilizer. *Environ. Prog. Sustain. Energy* **35**, 936–941 (2016).
- Özdemir, S., Sukatar, A. & Öztekin, G. Production of *Chlorella vulgaris* and its effects on plant growth, yield and fruit quality of organic tomato grown in greenhouse as biofertilizer. *Tarim. Bilim. Derg.* **22**, 596–605 (2016).
- García-González, J. & Sommerfeld, M. Biofertilizer and biostimulant properties of the microalga *Acutodesmus dimorphus*. *J. Appl. Phycol.* **28**, 1051–1061 (2016).
- Hernandez Melchor, D. J. *et al.* Phylogenetic and morphological identification of a photosynthetic microbial consortium of potential biotechnological interest. *Hidrobiológica* **26**, 311–321 (2016).
- Win, T. T. *et al.* Algal biofertilizers and plant growth stimulants for sustainable agriculture. *Ind. Biotechnol.* **14**, 203–211 (2018).
- Sangha, J. S. *et al.* Seaweeds (macroalgae) and their extracts as contributors of plant productivity and quality: The current status of our understanding. *Adv. Bot. Res.* **71**, 189–219 (2014).
- Tantawy, S. T. & Atef, N. M. Growth responses of *Lupinus termis* to some plant growth promoting cyanobacteria and bacteria as biofertilizers. *J. Food Agric. Environ.* **8**, 1178–1183 (2010).
- Win, T. T., Khan, S. & Fu, P. Fungus- (*Alternaria* sp.) mediated silver nanoparticles synthesis, characterization, and screening of antifungal activity against some phytopathogens. *J. Nanotechnol.* **2020**, 8828878 (2020).
- Oluwaseun, A. C. & Sarin, N. B. Impacts of biogenic nanoparticle on the biological control of plant pathogens. *Pollut. Res.* **24**, 13700–13709 (2017).
- Shah, M. *et al.* Green synthesis of metallic nanoparticles via biological entities. *Materials* **8**, 7278–7308 (2015).
- Tang, Z.-X. & Lv, B.-F. MgO nanoparticles as antibacterial agent: preparation and activity. *Braz. J. Chem. Eng.* **31**, 591–601 (2014).
- Smith, P. E. *et al.* Measurement of protein using bicinchoninic acid. *Anal. Biochem.* **150**, 76–85 (1985).
- Kaur, C. & Kapoor, H. C. Anti-oxidant activity and total phenolic content of some Asian vegetables. *Int. J. Food Sci. Technol.* **37**, 153–161 (2002).
- Stampoulis, D. *et al.* Assay-dependent phytotoxicity of nanoparticles to plants. *Environ. Sci. Technol.* **43**, 9473–9479 (2009).
- Abdul-Baki, A. A. & Anderson, J. D. Vigour determination in soybean by multiple criteria. *Crop Sci.* **10**, 31–34 (1973).
- Tripathi, R. *et al.* *Trichoderma koningii* assisted biogenic synthesis of silver nanoparticles and evaluation of their antibacterial activity. *Adv. Nat. Sci. Nanosci. Nanotechnol.* **4**, 035005 (2013).
- El Mel, A. A. *et al.* Creating nanoporosity in silver nanocolumns by direct exposure to radio-frequency air plasma. *Nanoscale* **8**, 141–148 (2016).
- El-Kassas, H. Y. & Ghobrial, M. G. Biosynthesis of metal nanoparticles using three marine plant species: Anti-algal efficiencies against *Oscillatoria simplicissima*. *Environ. Sci. Pollut. Res.* **24**, 7837–7849 (2017).
- Shankamma, K. *et al.* Fe₃O₄ magnetic nanoparticles to enhance *S. lycopersicum* (tomato) plant growth and their biomineralization. *Appl. Nanosci.* **6**, 983–990 (2016).
- Plaksenkova, I. *et al.* Effects of Fe₃O₄ nanoparticle stress on the growth and development of rocket eruca sativa. *J. Nanomater.* **2019**, 1–10 (2019).
- Polischuk, S. *et al.* The stimulating effect of nanoparticle suspensions on seeds and seedlings of Scotch pine (*Pinus sylvestris*). In *IOP Conference Series: Earth and Environmental Science* (IOP Publishing, 2019).
- Gonzalez-Melendi, P. *et al.* Nanoparticles as smart treatment-delivery systems in plants: assessment of different techniques of microscopy for their visualization in plant tissues. *Ann. Bot.* **101**, 187–195 (2008).
- Zhu, H. *et al.* Uptake, translocation, and accumulation of manufactured iron oxide nanoparticles by pumpkin plants. *J. Environ. Monit.* **10**, 713–717 (2008).
- Parveen, S. *et al.* Preparation, characterization and antifungal activity of iron oxide nanoparticles. *Microb. Pathog.* **115**, 287–292 (2018).
- Nehra, P. *et al.* Antibacterial and antifungal activity of chitosan coated iron oxide nanoparticles. *Br. J. Biomed. Sci.* **75**, 13–18 (2018).
- Loh, K.-S. *et al.* Use of Fe₃O₄ nanoparticles for enhancement of biosensor response to the herbicide 2, 4-dichlorophenoxyacetic acid. *Sensors* **8**, 5775–5791 (2008).
- Wang, X. *et al.* Uniform Fe₃O₄ microflowers hierarchical structures assembled with porous nanoplates as superior anode materials for lithium-ion batteries. *Appl. Surf. Sci.* **389**, 240–246 (2016).
- Khan, S. *et al.* Concurrent biomineralization of silver ions into Ag⁰ and Ag₂O by *Leptolyngbya* strain JSC-1 and the establishment of its axenic culture. *Chemosphere* **215**, 693–702 (2019).
- Rajeshkumar, S. *et al.* Seaweed-mediated synthesis of gold nanoparticles using *Turbidaria conoides* and its characterization. *J. Nanostruct. Chem.* **3**, 1–7 (2013).

Acknowledgements

TTW, BB, SZ and PCF are thankful to the financial support by the Research Start-Up Funds from Hainan University in China (KYQD_ZR2017212). SK is grateful for the support by Shaheed Benazir Bhutto University, Pakistan.

Author contributions

T.T.W. designed, performed the research. S.Z. performed the characterization experiment, T.T.W., B.B. and S.K. wrote the manuscript. P.C.F. supervised the research work and manuscript writing. All authors read and approved the final manuscript.

Competing interests

The authors declare no competing interests.

Additional information

Correspondence and requests for materials should be addressed to P.F.

Reprints and permissions information is available at www.nature.com/reprints.

Publisher's note Springer Nature remains neutral with regard to jurisdictional claims in published maps and institutional affiliations.



Open Access This article is licensed under a Creative Commons Attribution 4.0 International License, which permits use, sharing, adaptation, distribution and reproduction in any medium or format, as long as you give appropriate credit to the original author(s) and the source, provide a link to the Creative Commons licence, and indicate if changes were made. The images or other third party material in this article are included in the article's Creative Commons licence, unless indicated otherwise in a credit line to the material. If material is not included in the article's Creative Commons licence and your intended use is not permitted by statutory regulation or exceeds the permitted use, you will need to obtain permission directly from the copyright holder. To view a copy of this licence, visit <http://creativecommons.org/licenses/by/4.0/>.

© The Author(s) 2021